Inorganic Chemistry

Article

pubs.acs.org/IC

$[V_{16}O_{38}(CN)]^{9-}$: A Soluble Mixed-Valence Redox-Active Building Block with Strong Antiferromagnetic Coupling

Tony D. Keene,[†] Deanna M. D'Alessandro,[†] Karl W. Krämer,[‡] Jason R. Price,[†] David J. Price,[†] Silvio Decurtins,[‡] and Cameron J. Kepert*,[†]

[†]School of Chemistry, The University of Sydney, Sydney, New South Wales 2006, Australia

[‡]Departement für Chemie und Biochemie, Universität Bern, Freiestrasse 3, CH-3012 Bern, Switzerland

Supporting Information

ABSTRACT: A new discrete $[V_{16}O_{38}(CN)]^{9-}$ cluster, which displays the hitherto unknown 8− charge on the cluster shell and is the first to encapsulate the cyanide anion, has been synthesized and characterized by IR and UV/vis/near-IR spectroscopy, electrochemistry, and magnetic susceptibility measurements. Bond valence sum calculations conducted on the basis of the crystal structure analysis of $K_9[V_{16}O_{38}(CN)]\cdot 13H_2O$ confirm that this new member of the polyoxovanadate series is a mixed-valence complex. The intervalence charge transfer bands arising from intrametal interactions reveal that a localized (class II) assignment is appropriate for the cluster; however, a small degree of electronic delocalization is present. Interesting possibilities exist for the incorporation of this unit into higher dimensionality framework structures, where the redox, optical, and magnetic properties can be exploited and tuned.

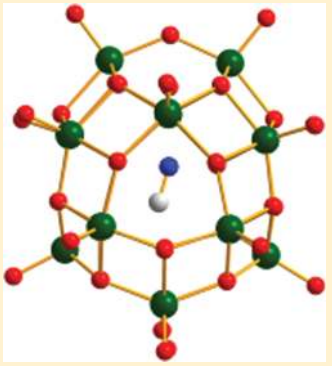

INTRODUCTION

Polyoxometalates have attracted significant interest in recent years in areas as diverse as medicine,[1] magnetism,[2] water splitting,[3] catalysis,[4] separation science,[5] computing,[6] and many others.[7] Much of this research has been focused on molybdates and tungstates, but vanadates also exhibit a wide range of structures and properties.[8]

The cluster-like topologies of polyoxovanadates endow them with excellent capabilities for encapsulating neutral and anionic species, which influence the size and shape of the clusters. A variety of cluster architectures have been observed, with a few groups being most prevalent in terms of their frequency of formation, such as $[V_{15}O_{36}]^{n-}$,[9] $[V_{15}O_{42}]^{n-}$,[10] and $[V_{18}O_{42}]^{n-}$ [11,10b] clusters. A smaller but equally interesting group is based on the $[V_{16}O_{38}(X)]^{n-}$ cluster.

The $[V_{16}O_{38}X]^{n-}$ cage has been observed in several works to date,[12−27] with charges of 12−,[12] 11−,[13] 7−,[14−22] 6−,[23] 5−,[24,25] and 3−[26,27] on the cluster shell and with X = F^-, Cl^-, Br^-, H_2O encapsulated within the cluster (Table 1). This diverse range of oxidation states is remarkable, considering that the cluster topology is maintained in each case. The majority of these clusters encapsulate the chloride anion and they exist as discrete anions[12] and also as metal−organic frameworks[13−27] on coordination to a secondary metal and bridging ligands.

As shown by Dong et al.,[21] these clusters can be redox-active and display reversible reduction and oxidation waves in acidified solution. This redox activity endows the compounds with interesting possible capabilities as semiconductors and battery materials if combined with suitable counterions in frameworks. The magnetic properties of several compounds have been studied and show a range of behaviors depending on the oxidation state of the cluster. A few cluster compounds such as those comprising the Lindqvist structure $[V_6O_{19}]^{n-}$ [28] have been found to exist in mixed-valence form, and the investigation of their intervalence charge transfer (IVCT) properties has revealed localized (Robin and Day class II[29]) behavior in the $V^{IV/V}$ mixed-valence species. Despite their rich mixed-valence properties, however, IVCT in higher nuclearity cluster compounds has seldom been probed, despite the potential of such measurements to provide one of the most powerful probes for intramolecular electron transfer.[30]

In this article, we present a new discrete $[V_{16}O_{38}(CN)]^{9-}$ cluster, which displays the hitherto unknown 8− charge on the cluster shell and is the first to encapsulate the cyanide anion. The results obtained from IR and UV/vis/near-IR spectroscopy, electrochemistry, magnetic susceptibility measurements, and bond valence sum calculations conducted on the basis of the crystal structure analysis reveal the interesting properties of this new member of the polyoxovanadate series.

RESULTS AND DISCUSSION

Structure of 1. Compound **1**[31] was synthesized by slow addition of MeOH to a filtered 4:1 solution of KCN:$VOSO_4\cdot 5H_2O$ in H_2O (full experimental details are given in the Supporting Information). The structure (Figure 1) consists of a $[V_{16}O_{38}(CN)]$ cluster with 9 potassium atoms and 13 water molecules, 2 of which are disordered over 2 sites. The cluster in **1** takes the form of an icosioctahedron (16 vertices, 28 faces,

Received: January 24, 2012

   dx.doi.org/10.1021/ic3001834 | Inorg. Chem. XXXX, XXX, XXX−XXX

Table 1. $V_{16}O_{38}$ Clusters from the Literature

compound	shell charge[a]	encapsulated moiety	V(IV):V(V)	ref
$K_{10}[H_2V_{16}O_{38}]\cdot 13H_2O$	12−	none	16:0	12
$\{[Cu(H_2O)(C_5H_{14}N_2)_2]_2[V_{16}O_{38}(Cl)]\}\cdot 4C_5H_{16}N_2$	11−	Cl^-	15:1	13
$K_9[V_{16}O_{38}(CN)]\cdot 13H_2O$	8−	CN^-	12:4	this work
$[\{Cu(1,2\text{-pn})_2\}_7\{V_{16}O_{38}(H_2O)\}_2]\cdot 4H_2O$	7−	H_2O	11:5	14
$Ni(en)_3\{[V_{16}O_{38}(Cl)][Ni(en)_2]_3\}\cdot 8.5H_2O$	7−	Cl^-	11:5	15
$[NH_4]_2[Zn(phen)_3]_2[Zn(phen)_2(H_2O)_2][V_{16}O_{38}(Cl)]\cdot 5H_2O$	7−	Cl^-	11:5	16
$H_2[C(CH_2OH)_3NH_3]_{1/2}[Cd(phen)_3]\{[Cd(H_2O)(phen)_2]_2(V_{16}O_{38}Cl)\}_{1/2}\{[Cd(H_2O)(phen)_2]_2(V_{16}O_{39}Cl)\}_{1/2}\cdot 2H_2O$	7−	Cl^-	11:5	17
$H_3[L/D\text{-}Cd(Cl)(H_2O)(phen)_2][\{L/D\text{-}Cd(H_2O)(phen)_2\}_2\{V_{16}O_{38}(Cl)\}]\cdot 3.5H_2O$	7−	Cl^-	11:5	18
$[Cu(2,2'\text{-bpy})_3]_2[H_4V_{16}O_{38}(Cl)]\cdot 4H_2O$	7−	Cl^-	11:5	19
$(bpy)[Co(4,4'\text{-bpy})_2]_2[H_4V_{16}O_{38}(Cl)]\cdot 6H_2O$	7−	Cl^-	11:5	20
$(bpy)[Zn(4,4'\text{-bpy})_2]_2[H_4\ V_{16}O_{38}(Cl)]\cdot 6H_2O$	7−	Cl^-	11:5	20
$H_2[Cd(phen)_3]_2\{[Cd(H_2O)(phen)_2][V_{16}O_{38}(Cl)]\}\cdot 2.5H_2O$	7−	Cl^-	11:5	21
$H_2[Cd(bpy)_3]_2\{[Cd(H_2O)(bpy)_2][V_{16}O_{38}(Cl)]\}\cdot 2.5H_2O$	7−	Cl^-	11:5	21
$[V_{16}O_{38}(Cl)][Cu(enMe)_2]_{7/2}\cdot 2H_2O$	7−	Cl^-	11:5	22
$[NiL]_3[V_{16}O_{38}(H_2O)]\cdot 6H_2O$	6−	H_2O	10:6	23
$[Cu(bbi)]_6[V_{16}O_{38}(Cl)]$	5−	Cl^-	9:7	24
$[Ni(en)_2(H_2O)_2[Ni(en)_3]_2[V_{16}O_{38}(Cl)]\cdot 3H_2O$	5−	Cl^-	9:7	25
$[Ni(4,4'\text{-bpy})_2]_2[V_{16}O_{38}(Cl)](4,4'\text{-bpy})\cdot 6H_2O$	3−	Cl^-	7:9	26
$[Ni(4,4'\text{-bpy})_2]_2[V_{16}O_{38}(F)](4,4'\text{-bpy})_{3/2}\cdot 3H_2O$	3−	F^-	7:9	27
$[Ni(4,4'\text{-bpy})_2]_2[V_{16}O_{38}(Br)](4,4'\text{-bpy})_{3/2}\cdot 3.5H_2O$	3−	Br^-	7:9	27
$[Co(4,4'\text{-bpy})_2]_2[V_{16}O_{38}(Cl)](4,4'\text{-bpy})_{3/2}\cdot 2H_2O$	3−	Cl^-	7:9	27
$[Mn(4,4'\text{-bpy})_2]_2[V_{16}O_{38}(Cl)](4,4'\text{-bpy})\cdot 2.5H_2O$	3−	Cl^-	7:9	27

[a]The shell charge refers to the charge on each cluster excluding that of any encapsulated species.

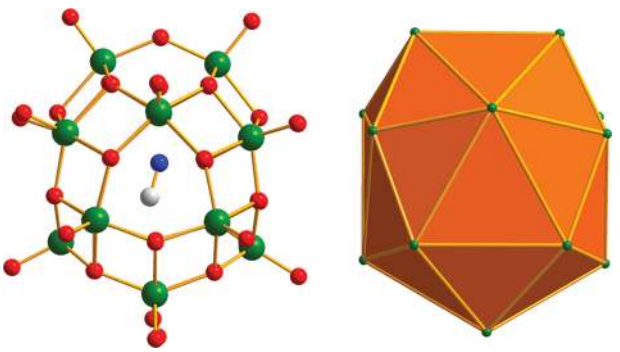

Figure 1. (a) $[V_{16}O_{38}(CN)]^{9-}$ cluster in **1** and (b) icosioctahedral cluster with D_{2d} symmetry.

and 42 edges)—a convex, nonregular deltahedron based on a hexagonal antiprism that is capped at each hexagonal face with two further vertices. Although there is no crystallographic symmetry element in the cluster, it is very close to being symmetrical, at which point it would have a point group of D_{2d} due to the two caps being aligned at 90° to each other. The cyanide anion is encapsulated within the cluster with average V···C and V···N distances of 3.287 and 3.339 Å, respectively, slightly closer than the sum of van der Waals radii. Each of the vanadium atoms is approximately square pyramidal with a square plane V−O distance of 1.932 Å and a V═O distance of 1.619 Å.

The clusters are surrounded by a complex sphere of potassium ions and water molecules. There is a degree of disorder to some of the water molecules, and in no cases were hydrogen atoms found from difference maps. Nonetheless, it is possible to see that the clusters are connected through a combination of hydrogen bonding and V═O−K−O═V interactions to build the three-dimensional structure (Figure 2). All V═O groups coordinate to potassium atoms (up to three in some cases), except O3, which appears to hydrogen bond to O7w, O3w, and O4w with O···O distances of 2.751(6), 3.206(7), and 3.467(6) Å, respectively.

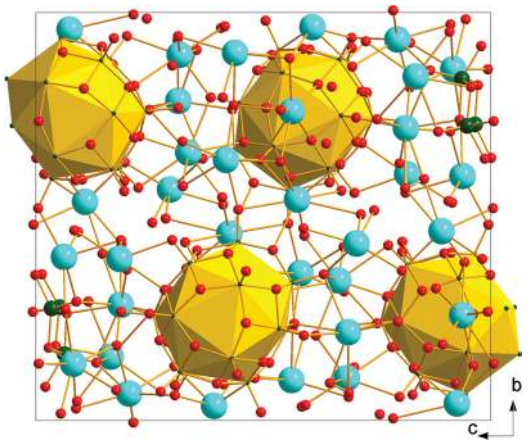

Figure 2. Packing diagram of **1** in a view down the *a* axis showing the complex network of potassium (light gray) and water (black) linking the clusters.

From the position of residual electron densities, it would appear that the cluster potentially has a small degree of disorder with two possible causes: (i) a very small fraction (too small to be reliably modeled) where the cluster is rotated 120° around the triangular aperture in the cluster—if this rotational disorder occurs, then the surrounding potassium and water sphere can maintain its position and still make reasonable interactions with the cluster or (ii) replacement of a small proportion of the $V_{16}O_{38}$ clusters by $V_{15}O_{36}$ clusters. The two cluster types are closely related in structure: if the apical oxygen atom is replaced

dx.doi.org/10.1021/ic3001834 | Inorg. Chem. XXXX, XXX, XXX−XXX

with a vanadyl unit and the two neighboring cap vanadyl units are deleted, then the $V_{15}O_{36}$ cluster arises, preserving the majority of the hydrogen-bonding network.

Assignment of Oxidation States. Other $V_{16}O_{38}$ clusters with the icosioctahedron structure have charges of 3−, 5−, 6−, 7−, 11−, or 12− (disregarding encapsulated anions), and in **1**, the charges of the surrounding cations and the cyanide anion indicate that there is a charge of 8−, which has not been seen before in this family. If the charge of 8− is correct for the $V_{16}O_{38}$ shell, then it is simple to calculate that there are 12 V^{IV} and 4 V^{V} centers, given the number of vanadium centers (16) and the sum of the charges on the vanadium atoms (68+).

As a check, we performed bond valence sum (BVS) calculations (eq 1)[32] for VO_5 centers using the +4 value for r_0 (1.784 Å):[33]

$$V = \sum \exp[(r_0 - r)/B] \quad (1)$$

where r_0 is an empirical value specific to the M−L bond examined, r is the M−L bond length, and B is an empirical value (0.37 for nearly all cases).

The results showed that in the cap V atoms (V_a), the BVS had an average of 4.42+ with 4.05+ for the second tier (V_b) and 4.26+ for the center (V_c), summing to 67.88+ for the cluster, remarkably close to the indicated value of 68+ for all 16 vanadium atoms. The cluster was separated into sections for this calculation, and in each case there was very little variation in the BVS for atoms within each group, so that atoms in similar environments have effectively the same charge density (Figure 3). This result indicates one of two possibilities: (i) the

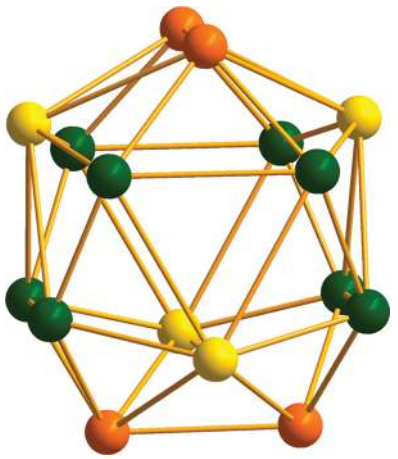

Figure 3. Oxidation states of the vanadium atoms in **1**: orange (V_a) denotes 4.5+, yellow (V_b) 4+, and green (V_c) 4.25+, summing to +68 over all 16 atoms, in accordance with the crystallographic structure.

cluster is crystallographically disordered so that localized charges are averaged on each site or (ii) that the charges in this cluster are partly delocalized, with one electron between the two cap atoms at each end (average 4.5+) and another two between the eight atoms of the middle tier (average 4.25+), while the second tier appears to be highly localized in the 4+ state. We investigate the second possibility further in this article. As a further check to ensure no undetected protons were attached to the cluster, BVS calculations on each of the bridging oxygen atoms revealed that they are all in the 2− state with values of 1.73−2.16 (values of 0−0.2 indicate H_2O, 0.8−1.2 HO^-, and 1.7−2.2 O^{2-}). Despite the potential disorder mentioned above, the atoms in the cluster are very well localized with small thermal displacement parameters; therefore, the BVS is valid in this case.

IR and UV/vis/Near-IR of 1. The solid state FT-IR spectrum of **1** shown in Figure 4 exhibits a strong absorption

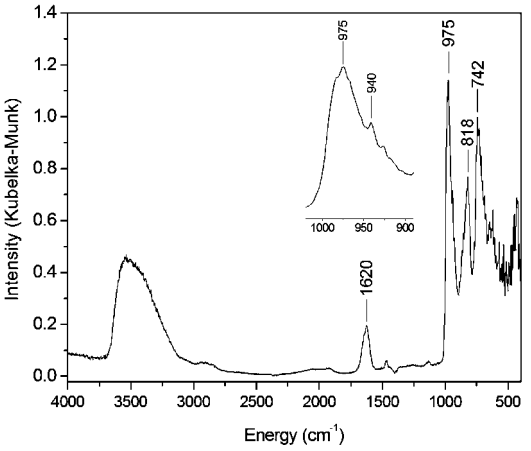

Figure 4. Solid-state FT-IR spectrum of **1** in KBr. The inset shows the $\nu(V{=}O_t)$ region.

band at 975 cm^{-1} associated with the terminal V=O stretch, $\nu(V{=}O_t)$, and medium-strong features at 818 and 742 cm^{-1}, which are ascribed to $\nu(O{-}V{-}O)$ vibrations.[17,20,21] The pattern of bands in the region characteristic of $\nu(V{=}O_t)$ indicates the presence of V^{IV} sites: clusters which contain exclusively V^{IV} generally possess $\nu(V{=}O_t)$ bands in the range 970−980 cm^{-1}, while bands in the region 940−960 cm^{-1} are characteristic of V^{V}.[34] The observation of a strong absorbance in the 970−980 cm^{-1} region provides a useful diagnostic for the presence of V^{IV} centers; however, the broadness of this band on the lower energy side and the presence of a distinctive vibration at 940 cm^{-1} suggests the presence of a mixed-valence core. The broad band in the region 3100−3700 cm^{-1} is associated with the H_2O molecules. While free $C{\equiv}N^-$ exhibits a stretching frequency at 2080 cm^{-1},[35] the cluster is characterized by a band at 1620 cm^{-1}, which is ascribed to the encapsulated cyanido anion. The significant decrease in the frequency is suggestive of a reduction in the bond order from triple to approximately double, presumably due to coupling of the cyanido stretch with the metal cluster modes. To the best of our knowledge, no prior observation of such an appreciable shift in a cyanido stretching frequency has been reported. The FT-IR spectrum for the related dinuclear V^{V} complex $[V_2O_3(\text{sal-L-val})_2(H_2O)]$ (sal-L-val = *N*-salicylidene-L-valinate) revealed a strong band at 1624 cm^{-1}, which was ascribed to $\nu(C{=}N)$ for the ligand backbone (C=N was directly bound to the V=O center).[36] In the present case, it would appear that delocalization of the anionic charge on the encapsulated anion with the cluster through π-back-bonding interactions is of a magnitude similar to that experienced by an imide ligand directly bound to a V center.

The UV/vis/near-IR spectrum of **1** was measured in both the solution (D_2O) and solid state (diffuse reflectance) over the range 4000−30 000 cm^{-1}, where $F(R)$ represents the Kubelka−Munk transform in the latter case (Figure 5, Table 2). Both spectra are characterized by a broad absorption feature in the near-IR region between 4000 and 12 000 cm^{-1}, which is identified as an intervalence charge transfer (IVCT) band on

dx.doi.org/10.1021/ic3001834 | Inorg. Chem. XXXX, XXX, XXX−XXX

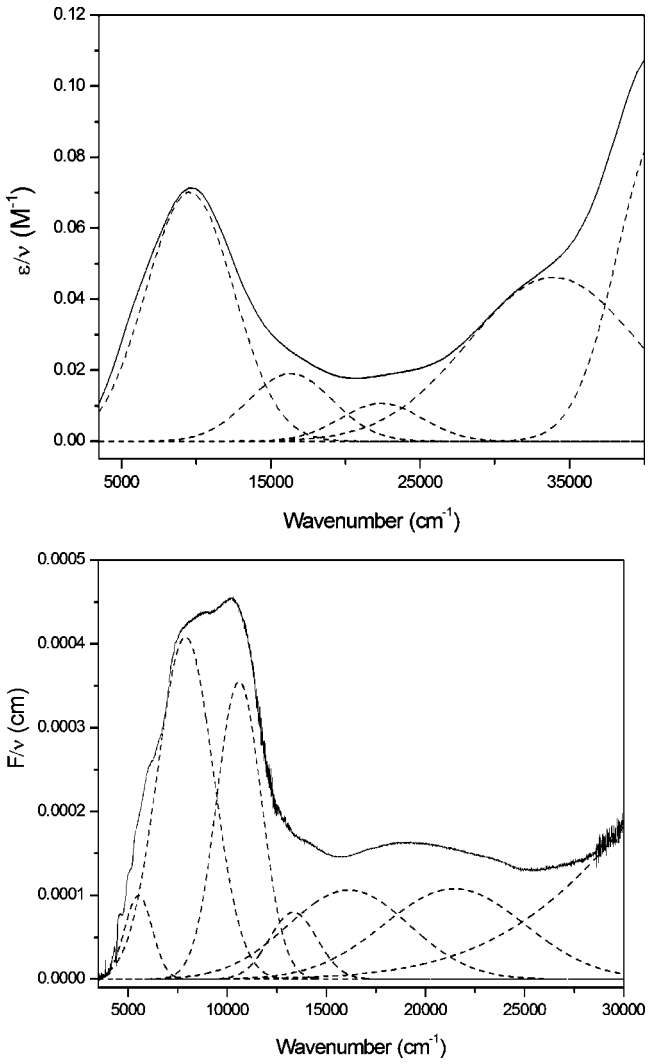

Figure 5. UV/vis/near-IR spectrum of **1** in D_2O (top) and as a solid (bottom). The dotted curves represent the best-fit Gaussian deconvolution.

Table 2. Solution and Solid-State Spectral Data of the Rescaled Absorption Spectra (ε/ν or F/ν vs ν) for 1[a]

Solution State (D_2O)			
ν_{max}/cm^{-1}	$(\varepsilon/\nu)_{max}/M^{-1}$	$\Delta\nu_{1/2}/cm^{-1}$	$\Delta\nu_{1/2}°/cm^{-1}$ [b]
9 683	**0.071 38**	**8 566**	**4 730**
9 590	0.070 29	6 920	4 706
16 335	0.019 12	6 618	6 142
22 413	0.010 74	6 420	
33 918	0.046 16	13 392	
Solid State			
ν_{max}/cm^{-1}	$(F/\nu)_{max} \times 10^{-4}$	$\Delta\nu_{1/2}/cm^{-1}$	$\Delta\nu_{1/2}°/cm^{-1}$ [b]
10 200	**4.55**	**6 445**	**4 854**
5 526	0.99	1 634	3 573
7 896	4.08	3 324	4 270
10 603	3.55	2 658	4 950
13 332	0.79	2 842	5 550
16 130	1.06	7 236	
21 459	1.08	8 363	

[a]The parameters in bold type are for the overall near-IR band manifolds (prior to deconvolution). [b]$\Delta\nu_{1/2}° = (2310\nu_{max})^{1/2}$ at 298 K.

the basis of a previous literature report for a mixed-valence $[V_6O_{19}]^{n-}$ cluster containing V^{IV}/V^{V} centers[28] and discrete dinuclear $[L(O)V^{IV}(\mu\text{-}O)V^{V}(O)L]^{-}$ mixed-valence compounds (where the two V atoms are linked linearly by O^{2-} and L is a ligand such as tris(2-pyridylmethyl)amine).[37] Since wavelength-dependent charge transfer intensities scale with the inverse of the absolute absorption energy (ν^{-1}),[30] the spectra are rescaled as F/ν or ε/ν vs ν (where ν is wavenumbers in cm^{-1}), for which Gaussian deconvolution reveals a number of transitions underlying the IVCT manifold. It must be noted that the energy maxima of IVCT bands in these reduced absorption spectra are identified with the vertical upper-/lower-surface energy separation and are the quantities most appropriately employed in the analysis of IVCT bands.[30]

The spectra in the visible and near-ultraviolet regions bear a strong resemblance to those of dinuclear $[L(O)V^{IV}(\mu\text{-}O)\text{-}V^{V}(O)L]^{-}$ compounds.[37] In the solution state, the band at 33 918 cm^{-1} is assigned to O→V ligand-to-metal charge transfer (LMCT); this band is evident at the limit of the spectral range in the solid state. The bands at 16 335 (312) and 22 413 cm^{-1} (240) in the solution state are attributed to d−d transitions which are observed in the ranges 13 000−14 100 and 16 600−17 900 cm^{-1} for mononuclear oxo complexes containing formally V^{IV} centers[37c] and dinuclear $[L(O)V^{IV}(\mu\text{-}O)V^{V}(O)L]^{-}$ compounds[37] (where the extinction coefficients in M^{-1} cm^{-1} are shown in parentheses). Two transitions within a similar range are also apparent at 16 130 and 21 459 cm^{-1} in the solid state with the possible assignment of an additional d−d transition at 13 332 cm^{-1}.

Intervalence Charge Transfer. A disparity in the appearance of the IVCT bands in the near-IR region of the solution and solid-state spectra is strikingly apparent. In the solution state, a broad Gaussian-shaped band centered at 9590 cm^{-1} (ε = 691 M^{-1} cm^{-1}) is observed. On the basis of the broader bandwidth at half-height, $\Delta\nu_{1/2}$, of 6920 cm^{-1} compared with that calculated from the classical theory of Hush[38] ($\Delta\nu_{1/2}$ = 4730 cm^{-1}), this band is characteristic of a localized (Robin and Day class II[29]) mixed valence compound (details of these calculations are provided in the Supporting Information). The classification here for class II compounds relates to the fact the two metal ions are distinguishable; however, some delocalization of the free electron does take place. Such class II compounds are distinguished from class III systems, in which the two metal ions are in exactly equivalent sites and the free electron is shared equally between the two metal ions.[29] Although the Hush model is strictly valid only for dinuclear mixed-valence complexes at the limits of class II and class III, its application would appear valid in the present case of the cluster, which itself lies in the weakly coupled regime.

Further evidence for localized behavior is apparent from the electronic matrix coupling element, H_{ab}, where $2H_{ab}$ provides a measure of the splitting between the lower and upper potential energy surfaces.[30] From the calculated value of 1350 cm^{-1} for H_{ab} (see the Supporting Information), $\nu_{max} > 2H_{ab}$, which provides further confirmation that the IVCT transition is localized and that a class II classification for the system is appropriate.

In the solid state, the IVCT band appears to be split into two major underlying components at 7896 and 10 603 cm^{-1}, in addition to a minor component at 5526 cm^{-1} (absolute intensities not measured). In each case, the observed bandwidths are narrower than those predicted from Hush theory,[38] suggesting the presence of significant delocalization of

dx.doi.org/10.1021/ic3001834 | Inorg. Chem. XXXX, XXX, XXX−XXX

charge (see Table 2). The appearance of multiple bands, however, is consistent with a residual degree of valence localization in the solid state, as confirmed by BVS calculations, which identified three environments for the V ions: the four ions at the outermost caps of the cluster (denoted V_a) in Figure 3 possess average calculated charges of 4.5+ and the four ions (V_b) in the second tier possess charges of 4.0+, while the eight ions (V_c) in the central band possess charges of 4.25+. Metal−metal charge transfer interactions which lead to partial delocalization of charge must therefore be present for $V_a \leftrightarrow V_b$, $V_a \leftrightarrow V_c$, and $V_b \leftrightarrow V_c$. In each case, there are eight possible V−O−V interactions, with the $V_a \leftrightarrow V_b$ interaction having the greatest dipole moment change (0.5 based on the difference in charges from BVS calculations). The $V_a \leftrightarrow V_c$ and $V_b \leftrightarrow V_c$ interactions possess similar dipole moment changes of 0.25. On this basis the two major underlying components are tentatively assigned to the $V_a \leftrightarrow V_b$ interaction and the overlapping $V_a \leftrightarrow V_c$ and $V_b \leftrightarrow V_c$ interactions. Thus, it would appear that, in the solid state, discrete V−O−V interactions between crystallographically distinct centers are present and there is some delocalization of charge. Indeed, IR spectroscopic results suggested that the mixed-valence cluster is partly trapped on the fast IR time scale (10^{-13}−10^{-14} s),[39] where the V═O_t stretching band can be considered as a spectator vibration to the V−O−V interactions. Considering these results, it can be assumed that the valence trapping ensued in the solid state is caused by cooperative effects in the crystalline phase which arise from significant hydrogen-bonding and intercluster V═O−K−O═V interactions (in addition to packing and dipole interactions, magnetic ordering, etc.). The presence of valence localization in the solid state is known to be common among complexes incorporating the mixed-valence $V^{IV}V^{V}O_3$ core.[37] One further possibility that cannot be discounted to rationalize the multiple IVCT transitions and the observation of localization on the IR time scale is the presence of vibronic coupling in the IVCT processes for the cluster.

The apparent inconsistency between the extent of electronic delocalization in the solution and the solid state can be rationalized if the localization that gives rise to distinct IVCT processes in the latter is partly removed when the clusters are dispersed in aqueous solution.

Electrochemistry. The cyclic voltammogram of **1** at a glassy-carbon electrode in 0.1 M KCl in water at 20 mV s^{-1} is shown in Figure 6. On the forward potential sweep, three processes are apparent at ~240, ~470, and 688 mV vs Ag/Ag^+, while only two processes are discernible at ~455 and 146 mV on the reverse sweep. One further irreversible process appears at −666 mV and is tentatively assigned as a $V^{IV/III}$ reduction. The presence of three processes on the initial anodic sweep supports the presence of three crystallographically distinct metal sites (with valencies of 4+, 4.25+, and 4.5+ from BVS calculations) which successively undergo oxidation to V^V. The splitting between the processes suggests that the V centers interact electronically: if all sites were electronically equivalent and noninteracting, they would undergo oxidation simultaneously. The processes appear to be quasi-reversible, but a definitive assignment for the processes is not possible, as the third $V^{V/IV}$ reduction process is not observed on the return potential sweep.

The scan rate dependence of the redox potentials was investigated at 20, 50, 100, 200, and 500 mV s^{-1} (Figure S1, Supporting Information). As the scan rate increases, two of the peaks assigned to oxidation of the vanadium centers to V^V disappear, as does the peak tentatively assigned as reduction to V^{III}. Corresponding shifts in the oxidation processes to more anodic potentials and the reductive process to more cathodic potentials are also observed.

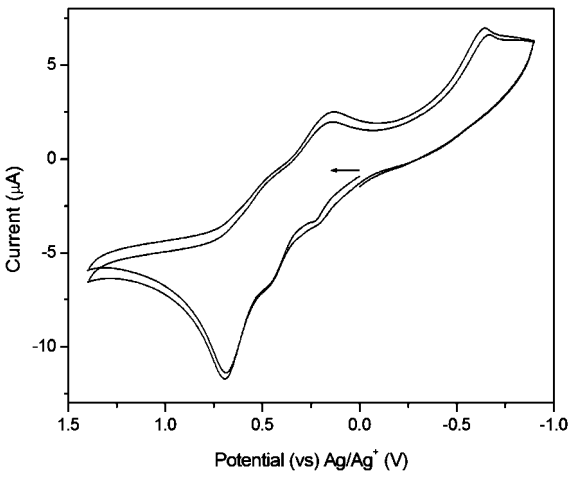

Figure 6. Cyclic voltammogram (two cycles) of **1** in 0.1 M KCl/H_2O at 20 mV s^{-1}. The arrow shows the initial scan direction.

Magnetic Properties. The magnetic susceptibility of **1** (Figure 7) shows an increasing value on cooling from 5.4 × 10^{-3} cm^3 mol^{-1} at 300 K, reaching a sharp maximum of 121 × 10^{-3} cm^3 mol^{-1} at 2.25 K before decreasing rapidly. The $\chi T(T)$ plot shows a value of 1.63 cm^3 K mol^{-1} at 300 K that decreases upon cooling. The decrease in value becomes sharper below 50 K, and a feature is seen with a minimum at 4.3 K, followed by a small increase and a very sharp decrease at 2 K, dropping to a value of 0.09 cm^3 K mol^{-1} at 1.9 K (the lowest measured temperature). The value of χT at 300 K is well below that expected for 12 noninteracting $S = {}^1/_2$ centers: g values for V^{IV} are usually isotropic with $g \approx 1.98$, which would give a value of 4.5 cm^3 K mol^{-1}. This implies that a strong antiferromagnetic interaction dominates in **1**. A Curie−Weiss model was not attempted, as this usually requires that fitting be done on an inverse susceptibility plot at temperatures well above the interaction strength.

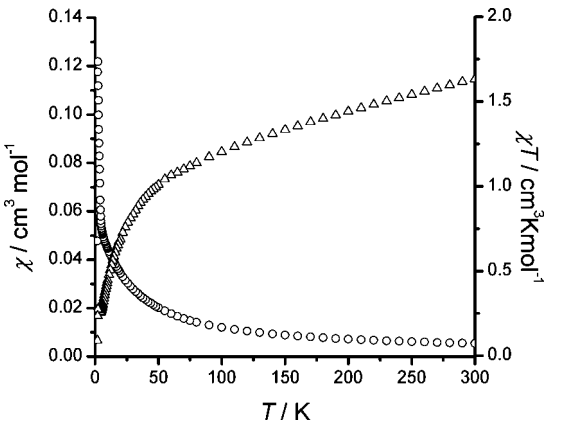

Figure 7. Magnetic susceptibility (○, left axis) and $\chi T(T)$ (△, right axis) plots for **1**.

In the case where the electrons in **1** were localized, there are 16 possible configurations. However, as seen in the UV/vis/

dx.doi.org/10.1021/ic3001834 | Inorg. Chem. XXXX, XXX, XXX−XXX

near-IR and BVS, they are delocalized, greatly complicating the interpretation of the susceptibility. Additionally, $V^{IV}-(O)_2-V^{IV}$ couplings can be highly variable, with only small changes in the pathway structural parameters.[40] However, a few points may be drawn from the data. As mentioned above, there is clearly a strong antiferromagnetic interaction dominant in **1**. The feature at 4.3 K shows a small increase in χT before dropping sharply, indicating a small ferromagnetic interaction before an ordering process occurs. In three-dimensionally ordered antiferromagnets, $\chi_{T=0}/\chi_{T=T_c} = {}^2/_3$,[41] whereas in **1** this ratio is considerably smaller and could appear to indicate potential metamagnetism. However, the magnetization plot (Figure S2, Supporting Information) does not support this, as the expected step in the curve at low field is not seen.

It is likely that the ordering process is facilitated by weak through-space interactions between the clusters.

Comparison with the other $V_{16}O_{38}$ clusters provides a very broad agreement between oxidation number and magnetic properties: for compounds with lower oxidation states (ref 13 and this work) the interactions appear to be antiferromagnetic, for "midrange" states ferro-[15] and antiferromagnetic[20] interactions can be seen, and in higher oxidation states only ferromagnetic interactions are seen.[26,27]

Discussion. The first report of a $V_{16}O_{38}$ cluster[12] dates from 2003, although several subsequent publications claim the first occurrence. In the following decades, clusters of this general type have been reported regularly by a small number of groups and various properties have been investigated, such as their electrochemical, magnetic, and structural characteristics, although no combined magnetic and electrochemical study has been undertaken to date.

Except for one other previously reported $V_{16}O_{38}$ cluster, they have been synthesized hydrothermally in conjunction with other metals and chelating groups. This greatly increases the complexity of designing functional systems, as a number of cluster types can be formed under very similar conditions. Several of the clusters have required reagents that are not incorporated into the structure during the synthesis, greatly complicating the prediction of the structure. Compound **1** thus has excellent potential as a secondary building unit (SBU) due to its stability and solubility in aqueous media. The only other simple salt of a $V_{16}O_{38}$ cluster, $K_{10}[H_2V_{16}O_{38}]\cdot 13H_2O$,[12] is highly unstable in air and forms a V_{18} cluster upon standing in solution, limiting its usefulness as an SBU. Preliminary results of combining **1** with M^{2+} ions have resulted in fast-forming powders that are under further investigation.

To the best of our knowledge (including CSD, Scifinder, ICSD, and Internet searches using a wide variety of search terms), compound **1** is the first polyoxometalate to encapsulate cyanide.

IR, UV/vis/near-IR, and electrochemical measurements indicate that partial delocalization of charge is present in **1**, with IVCT bands providing a powerful probe for the extent of intramolecular electron transfer. Intriguing possibilities exist for the incorporation of this unit into higher dimensionality framework structures, where ensuing conductivity may be realized.

Meanwhile, the rich redox chemistry of this and other $V_{16}O_{38}$ clusters presents interesting possibilities for modulating the magnetic interactions through chemical oxidation; the higher oxidation states appear to produce ferromagnetic interactions, while lower oxidation states are often antiferromagnetic. As such, a porous system containing these units could potentially be used as a sensor for oxidants or reductants through switching of the magnetic response.

CONCLUSIONS

We have synthesized a soluble, redox-active polyoxovanadate cluster with a new oxidation state which is the first of its type to encapsulate the cyanide anion. This material shows promise as a building block from which to construct new framework structures in a rational manner under ambient conditions, as it is water-soluble and stable in aqueous solution for at least 24 h. The reversible redox processes, coupled with the multiple oxidation states for the cluster, demonstrate that it is an excellent candidate for study as a battery material, an investigation of which we are currently undertaking.

EXPERIMENTAL SECTION

Experimental Methods. Synthesis was performed using commercially purchased reagents that were used without further purification. Single-crystal data were collected on a Bruker-Nonius FR591 Kappa Apex II diffractometer at 150 K using Mo Kα radiation (λ = 0.710 73 Å). Empirical absorption corrections were applied using SADABS.[42] The initial structure solution was obtained using SIR-92[43] and refined with SHELXL97[44] in the WinGX environment.[45] Magnetic susceptibility measurements were made using a Quantum Designs MPMS-5XL SQUID magnetometer. Susceptibility measurements were made in an applied field of 0.1 T between 300−1.9 K. Magnetisation measurements were made at 2 K (see Figure S2, Supporting Information) in fields of 0−5 T.

IR spectra were recorded on a Varian 800 Fourier transform infrared spectrometer using a KBr reference. Solution (D_2O) and solid-state UV/vis/near-IR spectra were recorded using a CARY 5E UV/vis/near-IR spectrophotometer which was interfaced to Varian WinUV software. In the case of solid-state measurements, the sample was mounted onto a high-density filter paper onto which an Omni Diff Probe attachment was placed. Two measurements were recorded per sample and averaged to reduce noise. Spectral deconvolution was performed using the curve-fitting subroutine implemented within the GRAMS32 commercial software package. The positions of the underlying bands were estimated by examining the first-order derivative of the spectrum as a guide to the energies of the major components; these were subsequently fixed, and the spectral deconvolution procedure was performed to obtain the parameters for the band intensities and bandwidths. The fixed parameters were successively removed as the fit was iteratively refined. Deconvolution was performed with the minimum number of components required to obtain convergence of the fitting procedure.

Solid-state electrochemical measurements were performed under argon using a BASi Epsilon Electrochemical Analyzer. Cyclic voltammograms were recorded under argon in 0.1 M KCl dissolved in water at 25 °C using a glassy-carbon working electrode, a platinum-wire auxiliary electrode, and an Ag/Ag^+ wire reference electrode.

Synthesis of 1. $VO(SO_4)\cdot 5H_2O$ (506 mg, 2.00 mol) was dissolved in a solution of KCN (521 mg, 8 mmol in 20 mL of H_2O) and stirred. The dark green solution (pH 10) was filtered and methanol slowly added to produce small greenish black crystals, which were washed with methanol and ether and dried under suction. Yield: 230 mg, 89% (based on V).

ASSOCIATED CONTENT

Supporting Information

Tables, text, figures, and a CIF file giving full experimental and synthetic details, bond distances and angles, detailed analysis of the UV/vis/near-IR data, calculation of the electronic matrix coupling element, a magnetization plot, cyclic voltammograms and crystal data for **1**. This material is available free of charge via the Internet at http://pubs.acs.org.

dx.doi.org/10.1021/ic3001834 | Inorg. Chem. XXXX, XXX, XXX−XXX

AUTHOR INFORMATION

Corresponding Author

*Fax: (+61) 2 9351-3329. E-mail: cameron.kepert@sydney.edu.au.

Notes

The authors declare no competing financial interest.

ACKNOWLEDGMENTS

C.J.K. and D.M.D. acknowledge the support of The University of Sydney and the Australian Research Council. This work was also supported by the Swiss National Science Foundation (Grant No. 200020-130266).

REFERENCES

(1) (a) Altirriba, J.; Barbera, A.; Del Zotto, H.; Nadal, B.; Piquer, S.; Sánchez-Pla, A.; Gagliardino, J. J.; Gomis, R. *BMC Genomics* **2009**, *10*, 406. (b) Rhule, J. T.; Hill, C. L.; Judd, D. A.; Schinazi, R. F. *Chem. Rev.* **1998**, *98*, 327−358. (c) Aureliano, M.; Crans, D. C. *J. Inorg. Biochem.* **2009**, *103*, 536−546. (d) Hill, C. L.; Weeks, M.; Hartnup, M.; Sommadossi, J.-P.; Schinazi, R. F. *Ann. N.Y. Acad. Sci.* **1990**, *616*, 528−529.

(2) (a) Müller, A.; Luban, M.; Schröder, C.; Modler, R.; Kögerler, P.; Axenovich, M.; Schnack, J.; Canfield, P.; Bud'ko, S.; Harrison, N. *ChemPhysChem* **2001**, *2*, 517−521. (b) Müller, A.; Peters, F.; Pope, M. T.; Gatteschi, D. *Chem. Rev.* **1998**, *98*, 239−272. (c) Casañ-Pastor, N.; Baker, L. C. W. *Mol. Eng.* **1993**, *3*, 141−155. (d) Barbour, A.; Luttrell, R. D.; Choi, J.; Musfeldt, J. L.; Zipse, D.; Dalal, N. S.; Boukhvalov, D. W.; Dobrovitski, V. V.; Katsnelson, M. I.; Lichtenstein, A. I.; Harmon, B. N.; Kögerler, P. *Phys. Rev. B* **2006**, *74*, 014411.

(3) (a) Yin, Q.; Tan, J. M.; Besson, C.; Geletii, Y. V.; Musaev, D. G.; Kuznetsov, A. E.; Luo, Z.; Hardcastle, K. I.; Hill, C. L. *Science* **2010**, *328*, 342−345. (b) Weinstock, I. A.; Barbuzzi, E. M. G.; Wemple, M. W.; Cowan, J. J.; Reiner, R. S.; Sonnen, D. M.; Heintz, R. A.; Bond, J. S.; Hill, C. L. *Nature* **2001**, *414*, 191−195. (c) Geletii, Y. V.; Botar, B.; Kögerler, P.; Hillesheim, D. A.; Musaev, D. G.; Hill, C. L. *Angew. Chem., Int. Ed.* **2008**, *47*, 3896−3899.

(4) (a) Kamata, K.; Yonehara, K.; Nakagawa, Y.; Uehara, K.; Mizuno, N. *Nat. Chem.* **2010**, *2*, 478−483. (b) Sadakane, M.; Steckhan, E. *Chem. Rev.* **1998**, *98*, 219−238. (c) Kozhevinikov, I. V. *Catalysis by Polyoxometalates*; Wiley: Chichester, U.K., 2002.

(5) (a) Jeppsson, L.; Anehus, R. *Alcheringa* **1999**, *23*, 57−62 and references therein. (b) Bolch, C. J. S. *Phycologia* **1997**, *36*, 472−478.

(6) Lehmann, J.; Gaita-Ariño, A.; Coronado, E.; Loss, D. *Nat. Nanotechnol.* **2007**, *2*, 312−317.

(7) See for example: (a) Katsoulis, D. E. *Chem. Rev.* **1998**, *98*, 359−388. (b) *Polyoxometalate Molecular Science*; Borrás-Almenar, J. J., Coronado, E., Müller, A., Pope, M., Eds.; Kluwer Academic: Dordrecht, The Netherlands, 2003; NATO Science Series II, Physics and Chemistry, Vol. *98*. (c) *Polyoxometalates: From Platonic Solids to Anti-retroviral Activity*; Pope, M. T., Müller, A., Eds.; Kluwer Academic: Dordrecht, The Netherlands, 1994.

(8) See for example: (a) Müller, A.; Rohlfing, R.; Krickemeyer, E.; Bögge, H. *Angew. Chem., Int. Ed. Engl.* **1993**, *32*, 909−912. (b) Livage, J.; Bouhedja, L.; Bonhomme, C. *J. Sol-Gel Sci. Tech.* **1998**, *13*, 65−70. (c) Bouhedja, L.; Steunou, N.; Maquet, J.; Livage, J. *J. Solid State Chem.* **2001**, *162*, 315−321. (d) Oyaizu, K.; Dewi, E. L.; Tsuchida, E. *J. Electroanal. Chem.* **2001**, *498*, 136−141. (e) Schoiswohl, J.; Surnev, S.; Netzer, F. P.; Kresse, G. *J. Phys.: Condens. Matter* **2006**, *18*, R1−R14.

(9) See for example: (a) Müller, A.; Krickenmeyer, E.; Penk, M.; Walberg, H.-J.; Bögge, H. *Angew. Chem., Int. Ed. Engl.* **1987**, *26*, 1045−1046. (b) Thomas, J.; Sharma, S.; Lofland, S. E.; Ramaujachary, K. V.; Ramanan, R. *J. Chem. Sci.* **2006**, *118*, 79−86. (c) Yamase, T.; Ohtaka, K. *J. Chem. Soc., Dalton Trans.* **1994**, 2599−2608. (d) Drezen, T.; Joubert, O.; Ganne, M.; Brohan, L. *J. Solid State Chem.* **1998**, *136*, 298−304. (e) Hayashi, Y.; Miyakoshi, N.; Shinguchi, T.; Uehara, A. *Chem. Lett.* **2001**, *30*, 170−171.

(10) See for example: (a) Khan, M. I.; Deb, S.; Aydemir, K.; Alwarthan, A. A.; Chattopadhyay, S.; Miller, J. T.; Marshall, C. L. *Catal. Lett.* **2010**, *135*, 282−290. (b) Pavani, K.; Upreti, S.; Ramanan, A. *J. Chem. Sci.* **2006**, *118*, 159−165.

(11) See for example: (a) Müller, A.; Sessoli, R.; Krickenmeyer, E.; Bögge, H.; Meyerm, J.; Gatteschi, D.; Pardi, L.; Westphal, J.; Hovemeier, K.; Rohlfing, R.; Döring, J.; Hellweg, F.; Beugholt, C.; Schmidtmann, M. *Inorg. Chem.* **1997**, *36*, 5239−5250. (b) Johnson, G. K.; Schlemper, E. O. *J. Am. Chem. Soc.* **1978**, *100*, 3645−3646. (c) Natarajan, S.; Narayan, K. S.; Pati, S. *J. Chem. Sci.* **2006**, *118*, 57−65.

(12) Long, D.-L.; Orr, D.; Seeber, G.; Kögerler, P.; Farrugia, L. J.; Cronin, L. *J. Cluster Sci.* **2003**, *14*, 313−324.

(13) Wutkowski, A.; Näther, C.; Speldrich, M.; Kögerler, P.; Bensch, W. *Z. Anorg. Allg. Chem.* **2009**, *635*, 1094−1099.

(14) Lin, B.-Z.; Liu, S.-X. *Chem. Commun.* **2002**, 2126−2127.

(15) Pan, C.-L.; Xu, J.-Q.; Li, G.-H.; Chu, D.-Q.; Wang, T.-G. *Eur. J. Inorg. Chem.* **2003**, 1514−1517.

(16) Chen, Y.; Gu, X.; Peng, J.; Shi, Z.; Yu, H.; Wang, E.; Hu, N. *Inorg. Chem. Commun.* **2004**, *7*, 705−707.

(17) Dong, B.; Chen, Y.; Peng, J.; Kong, Y.; Han, Z. *J. Mol. Struct.* **2005**, *748*, 171−176.

(18) Chen, Y.; Peng, J.; Yu, H.; Han, Z.; Gu, X.; Shi, Z.; Wang, E.; Hu, N. *Inorg. Chim. Acta* **2005**, *358*, 403−408.

(19) Dong, B.; Peng, J.; Chen, Y.; Kong, Y.; Tian, A. *J. Mol. Struct.* **2006**, *788*, 200−205.

(20) Dong, B.; Gómez-Garciá, C. J.; Peng, J.; Benmansour, S.; Kong, Y. *J. Mol. Struct.* **2007**, *827*, 50−55.

(21) Dong, B.; Peng, J.; Tian, A.; Sha, J.; Li, L.; Liu, H. *Electrochim. Acta* **2007**, *52*, 3804−3812.

(22) Cui, X.-B.; Zheng, S.-T.; Sun, Y.-Q.; Yang, G.-Y. *Chem. Res. Chin. Univ.* **2004**, *20*, 266−269.

(23) Ou, G.-C.; Jiang, L.; Feng, X.-L.; Lu, T.-B. *Dalton Trans.* **2009**, 71−76.

(24) Dong, B.-X.; Peng, J.; Gómez-Garciá, C. J.; Banmansour, S.; Jia, H.-Q.; Hu, N.-H. *Inorg. Chem.* **2007**, *46*, 5933−5941.

(25) Liu, X.; Yin, X.-H.; Zhang, F. *Z. Naturforsch.* **2010**, *65b*, 1451−1456.

(26) Liu, S.; Xie, L.; Gao, B.; Zhang, C.; Sun, C.; Li, D.; Su, Z. *Chem. Commun.* **2005**, 5023−5025.

(27) Zhang, C.-D.; Liu, S.-X.; Gao, B.; Sun, C.-Y.; Xie, L.-H.; Yu, M.; Peng, J. *Polyhedron* **2007**, *26*, 1514−1522.

(28) Daniel, C.; Hartl, H. *J. Am. Chem. Soc.* **2009**, *131*, 5101−5114.

(29) Robin, M. B; Day, P. *Adv. Inorg. Chem. Radiochem.* **1967**, *10*, 247−403.

(30) D'Alessandro, D. M.; Keene, F. R. *Chem. Soc. Rev.* **2006**, *35*, 424−440 and references therein..

(31) Crystal data for **1**: $CH_{26}K_9NO_{51}V_{16}$, 2035.13 g mol^{-1}, monoclinic, $P2_1/n$ (No. 14), 150 K, a = 11.3351(9) Å, b = 20.1302(16) Å, c = 22.5130(16) Å, β = 94.978(2)°, V = 5117.6(7) Å^3, Z = 4, ρ_{calcd} = 2.607 g cm^{-3}, μ = 3.622 mm^{-1}, λ = 0.710 73 Å (Mo Kα), $2\theta_{max}$ = 25.00°, 61 311 reflections measured (9012 unique, R_{int} = 0.0313), R1/wR2 ($2\sigma > I$) = 0.0459/0.1237 (7877 reflections), R1/wR2 (all data) = 0.0537/0.1329 (9012 reflections), residual electron density maximum 3.090 e Å^{-3} (see text for details) and minimum −1.817 e Å^{-3}, rms = 0.177 e Å^{-3}. CCDC reference number 837819.

(32) Brown, I. D.; Altermatt, D. *Acta Crystallogr.* **1985**, *B41*, 244−247.

(33) Brown, I. D.; http://www.ccp14.ac.uk/ccp/web-mirrors/i_d_brown/bond_valence_param/bvparm2006.cif, accessed 10/09/2010.

(34) Khan, M. I.; Chen, Q.; Goshorn, D. P.; Zubleta, J. *Inorg. Chem.* **1993**, *32*, 672−680.

(35) *Spectrometric Identification of Organic Compounds*, 5th ed.; Wiley: Hoboken, NJ, 1991.

(36) Cavaco, I.; Pessoa, J. C.; Duarte, M. T.; Henriques, R. T.; Matias, P. M.; Gillard, R. D. *J. Chem. Soc., Dalton Trans.* **1996**, 1989−1996.

(37) (a) Dinda, R.; Sengupta, P.; Ghosh, S.; Mak, T. C. W. *Inorg. Chem.* **2002**, *41*, 1684−1688. (b) Dutta, S.; Basu, P.; Chakravorty, A.

Inorg. Chem. **1993**, *32*, 5343−5348. (c) Holwerda, R. A.; Whittlesey, B. R; Nilges, M. J. *Inorg. Chem.* **1998**, *37*, 64−68. (d) Kojima, A.; Okazaki, K.; Ooi, S.; Saito, K. *Inorg. Chem.* **1983**, *22*, 1168−1174. (e) Mahroof-Tahir, M.; Keramidas, A. D.; Goldfarb, R. B.; Anderson, O. P.; Miller, M. M.; Crans, D. C. *Inorg. Chem.* **1997**, *36*, 1657−1668.
(38) Allen, G. C.; Hush, N. S. *Prog. Inorg. Chem.* **1967**, *8*, 357−389.
(39) Demadis, K. D.; Hartshorn, C. M.; Meyer, T. J. *Chem. Rev.* **2001**, *101*, 2655−2685 and references therein..
(40) See for example: Rodriguez-Fortea, A.; Llunell, M.; Alemany, P.; Canadell, E. *Inorg. Chem.* **2009**, *48*, 5779−5789 Table 1 and references therein..
(41) See for example: Carlin, R. L. *Magnetochemistry*; Springer-Verlag: Heidelberg, Germany, 1986.
(42) Sheldrick, G. M. *SADABS*; University of Göttingen, Göttingen, Germany, 1996.
(43) Altomare, A.; Cascarano, G.; Giacovazzo, C.; Guagliardi, A.; Burla, M. C.; Polidori, G.; Camalli, M. *J. Appl. Crystallogr.* **1994**, *27*, 435.
(44) Sheldrick, G. M. *Acta Crystallogr.* **2008**, *A64*, 112−122.
(45) Farrugia, L. J. *J. Appl. Crystallogr.* **1999**, *32*, 837−838.